Journal of the Mechanics and Physics of Solids 131 (2019) 344–357

Contents lists available at ScienceDirect

Journal of the Mechanics and Physics of Solids

journal homepage: www.elsevier.com/locate/jmps

Bandgap tuning in bioinspired helicoidal composites

Nicolás Guarín-Zapata[a], Juan Gómez[b], David Kisailus[c], Pablo D. Zavattieri[a,*]

[a] Lyles School of Civil Engineering, Purdue University, West Lafayette, IN 47907, USA
[b] Civil Engineering Department, Universidad EAFIT, Medellín 050022, Colombia
[c] Materials Science and Engineering and Department of Chemical and Environmental Engineering, University of California, Riverside, CA 92521, USA

ARTICLE INFO

Article history:
Received 16 March 2019
Revised 8 June 2019
Accepted 4 July 2019
Available online 6 July 2019

Keywords:
Fiber reinforced composites
Dispersion
Wave propagation
Bandgaps
Helicoidal composites
Biomimetics

ABSTRACT

The dispersion of waves in helicoidal layered composites is investigated using propagation matrices and the Bloch's theorem to represent the layered nature and periodicity of the material, respectively. Dispersion relations are found solving the resulting eigenvalue problems. Concrete numerical investigations are made for a collection of transversely isotropic materials. The influence of the anisotropy (or directionality) of the constituent materials for each layer is presented in a qualitative and quantitative fashion. Dispersion curves are presented for some of these materials, and for different helicoidal configurations. We determined the size of the first bandgap for different anisotropy levels, showing that the most important parameter for shear wave filtering is the ratio of elastic constants C_{44}/C_{66}, and thus the anisotropy of the S waves in each layer is more interesting than the anisotropy for quasi–S and quasi–P ones. Considering the results, we can design for the appearance and size of the bandgaps by careful selection of the materials that constitute the layers of the composites.

1. Introduction

It is well known that the overall behavior of heterogeneous materials is determined by mechanical and geometric properties of the constitutive microstructural features. This has impacted current guidelines in materials design which are not just based on changing the properties of the different phases but also on modifying its base architecture. Hence, the mechanical behavior of composite materials can be tailored by designing microstructures that alternate stiff and flexible constituents combined with well–designed architectures. Recent advances in materials fabrication technology and additive manufacturing have allowed the realization of materials with controlled architectures enabling new properties and functionalities (Babaee et al., 2013; Ge et al., 2013; Lin et al., 2014; Celli and Gonella, 2015; Porter et al., 2017; Slesarenko et al., 2017; Jasiuk et al., 2018; Akbari et al., 2018, Liang et al., 2018).

Currently, there is a strong interest in the research community to expand the material space by exploring novel microstructural architectures that take advantage of the response of independent phases (Ashby and Bréchet, 2003; Brechet and Embury, 2013). Two interesting examples correspond to transversely isotropic materials and helicoidal composites. Transversely isotropic materials are widely applied in many different fields like geophysics, crystal acoustics and composites (Backus, 1962; Musgrave, 1970; Nye, 1985; Slawinski, 2010; Dvorak, 2013). Among many interesting properties, these

* Corresponding author.
E-mail address: zavattie@purdue.edu (P.D. Zavattieri).

https://doi.org/10.1016/j.jmps.2019.07.003
0022-5096/

materials exhibit direction-dependent phase speed. Similarly, helicoidal composites have been shown to exhibit shear wave filtering capabilities by virtue of its periodic arrangement (Guarín–Zapata et al., 2015). Previous studies have also found, that layered composites in addition to wave filtering (Guarín–Zapata et al., 2015), also exhibit negative refraction (Willis, 2015) and near omnidirectional high-pass filtering (Srivastava, 2016). In particular, it was shown by Guarín–Zapata et al. (2015) that the extraordinary absorbing energy capabilities existing in the dactyl club of stomatopods can be partially attributed to the bouligand–like (helicoidal) structure present in its material microstructure. These findings, together with the independent behavior of the different phases, suggest that such remarkable energy absorption capabilities can be improved through optimal combinations of the base materials used in the composite, in addition to variations in the geometric properties defining the material cell. Although helicoidal composites and transversely isotropic materials have been studied extensively, its combined effect from a wave propagation point of view has not been fully investigated. This work is devoted to the exploration of the band structure of biomimetic helicoidal composites, like those found in the dactyl club of stomatopods, which are formed by an arrangement of stacked transversely isotropic layers. Such multilayer arrangements are a common motif in nature (Saheb et al., 1999) and in several engineered materials (Jones, 1975; Gibson, 2011).

In fact, many organisms are recognized for their capacity to produce materials with outstanding responses through a hierarchically–organized assembly of simple constituents (Wegst and Ashby, 2004; Barthelat, 2007; Meyers et al., 2013). Some of these components are fibrous, gradient, layered, tubular, cellular, suture, overlapping and helicoidal structures (Naleway et al., 2015, 2016). In particular, helicoidal composites are found frequently and have been identified as microstructural features in a variety of species, such as fish scales (Zimmermann et al., 2013), exoskeletons of beetles (Cheng et al., 2009), crabs (Chen et al., 2008), lobsters (Al-Sawalmih et al., 2008), dactyl clubs of stomatopods (Weaver et al., 2012; Guarín–Zapata et al., 2015; Yaraghi et al., 2016, Grunenfelder et al. 2018.), and mammalian bone collagen (Yamamoto et al., 2012). In all of these works, the general finding is that the presence of helicoidal arrangements can lead to an increase in toughness (Grunenfelder et al., 2014; Suksangpanya et al., 2017, 2018; Yaraghi et al., 2019; Shishehbor and Zavattieri, 2019; Huang et al., 2019) and filtering in shear waves (Guarín–Zapata et al., 2015).

Despite the relatively wide research efforts in the field of structural arrangements in biological materials, there are only a few works dealing with its characterization from the wave propagation perspective. The characterization of these materials under traveling mechanical perturbations can be conducted using numerical methods. For this purpose helicoidal composites can be modeled as periodic materials (or phononic crystals) where the unit of repetition is comprised of multiple layers exhibiting a 180° rotation resulting also in a periodic variation in the mechanical properties. Under these assumptions, phononic crystals are known to exhibit bandgaps, i.e., ranges of frequency where waves cannot propagate (Brillouin, 2003; Deymier, 2013). The structure analysis and determination of the resulting bandgaps for a specific material model can be achieved by nowadays standard methods based upon Bloch's theorem (Kittel and McEuen, 1986; Brillouin, 2003) and using as primary model that of a single fundamental material cell.

On the other hand, the idea of transverse isotropy has been used to model the overall behavior of materials reinforced by fibers aligned in the same direction, both in engineering and biological materials (Dvorak, 2013; Cheng et al., 2008, 2009; Cheng, 2010; Nikolov et al. 2010, 2011, Liu and Huang, 2012, Astaneh and Guddati, 2017, Liang et al., 2018, Thierry et al., 2018). Wave propagation in that class of materials is anisotropic, or directional, with the phase speed of the perturbation dependent upon the propagation direction. Although this is a well-known fact, we examine how the directionality effect modifies the wave filtering capability of helicoidal composites. Particularly, we study the dispersion of waves propagating in helicoidal composites where the constituent materials are transversely isotropic. The analysis is motivated by the remarkable wave absorption capabilities identified in the dactyl club of stomatopods and attributed partially to the helicoidal composite nature of its microstructure, and specifically to its periodic arrangement. As was concluded from previous investigations, the size of the bandgap (controlling the fraction of absorbed energy in the material), was a function of the pitch angle in the layered system. Here, we focus on the properties of the transversely isotropic base materials and evaluate its impact on the bandgap formation.

In the first part of the paper, we examine the wave directionality effect of transversely isotropic materials starting from standard expressions relating phase speed to propagation direction. The resulting expressions, which are also an equivalent representation of the constitutive response of the material, are subsequently presented in the form of phase-speed surfaces highlighting the directionality effect for the different modes. The section concerning transversely isotropic materials concludes with the selection of a quantitative measure or index to objectively describe the level of anisotropy in a given transversely isotropic material. This index is then used to comparatively describe a database of natural and man-made transversely isotropic materials. The second part of the paper focuses on the dispersion analysis of helicoidal composites whose constituent material is transversely isotropic. As a performance descriptor of the different combinations of material parameters and cell properties, we selected the gap–midgap ratio. The dispersion analysis was conducted using the propagator matrix approach together with Bloch periodic boundary conditions. To better quantify the performance of the resulting composites, we measure the amount of filtered energy assuming the material is excited with an input in the form of a square pulse. The final part of the paper presents some conclusions and recommendations for further work.

2. Wave directionality of transversely isotropic materials

There are two salient features in transversely isotropic media. First, the shear (S), quasi-shear (qS) and quasi-compressional (qP) propagation modes existing in these materials exhibit direction dependent phase velocities. Second, dif-

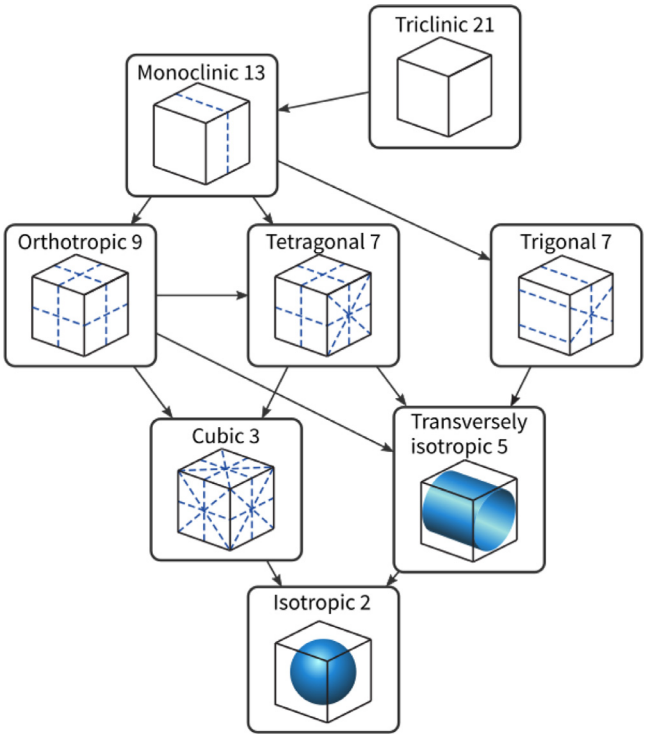

Fig. 1. Schematic for classes of material symmetry with planes of symmetry indicated by dashed lines. The emerging arrows represent different subgroups, while the number inside each box indicates the number of independent constants for each material symmetry. Based on (Moakher, 2009).

ferent combinations of the values of the constitutive parameters produce substantially different directional behavior. Such anisotropic wave propagation response creates the need for objective representations of the level of anisotropy associated with a specific material whenever the analysis is intended to identify wave propagation effective materials. Here, we first review some fundamental descriptors of the dispersive behavior of transversely isotropic media based upon a qualitative characterization of the constitutive tensor. The analysis is then complemented by a brief survey of quantitative measures or indices leading to the selection of an objective, mode-independent anisotropy index (AI). The identified qualitative and quantitative descriptors are then applied to a selected database of commonly used transversely isotropic materials. From this database, we further select a man-made and a natural material to be used as prototypes, and to use them in helicoidal architectures in order to explore wave attenuation improvement.

2.1. Transversely isotropic materials

Transversely isotropic materials possess mechanical properties which are symmetric about an axis while keeping isotropy inside the plane orthogonal to this axis. By contrast with purely isotropic materials, this transverse isotropy results in the appearance of shear (S), quasi-shear (qS) and quasi-compressional (qP) propagation modes whose phase velocities become direction dependent.

To contextualize transversely isotropic materials within general anisotropic behavior, we schematized (Fig. 1) different symmetry classes found in elastic materials. The description is organized hierarchically from top to bottom, specifying the number of elastic constants required in each constitutive tensor. The arrows indicate subgroups of a given class of symmetry. The case of a transversely isotropic material (with 5 constitutive parameters), is shown in the second row from the bottom. This structure corresponds to a cylinder whose axis of revolution specifies the axis of symmetry in the constitutive relation (Moakher, 2009). For completeness, we also show in the last row the simplest case of isotropic media corresponding to a sphere.

In wave propagation analysis, the constitutive response is better described in terms of dispersion relations that indicate phase velocities. We use standard computations, as in Carcione (2001), to arrive at the following dispersive description of an arbitrary transversely isotropic material for the qP, qS and S modes:

$$v_{\mathrm{qP}}(\theta) = \sqrt{\frac{C_{11}\sin^2(\theta) + C_{33}\cos^2(\theta) + C_{44} + \sqrt{M(\theta)}}{2\rho}},$$

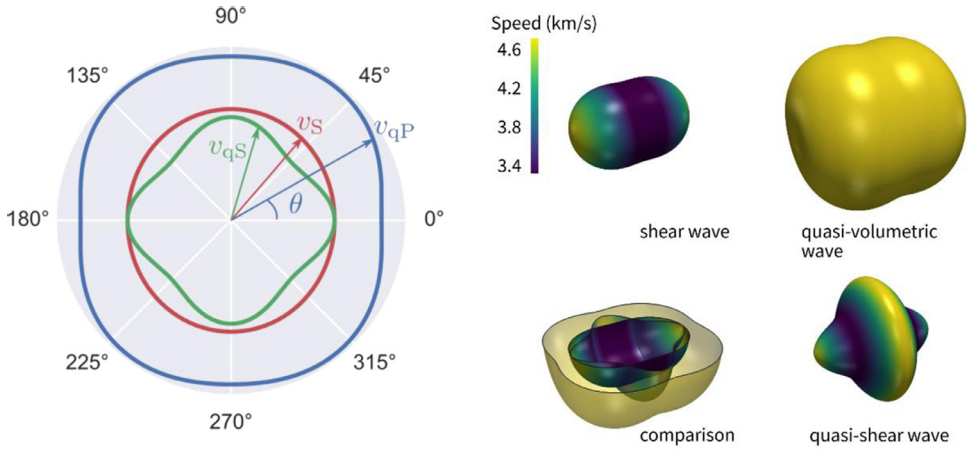

Fig. 2. (**Left**) Directionality of wave modes for a transversely isotropic material. The angle θ is measured with respect to the axis of symmetry. (**Right**) Phase speed for the different wave modes for magnesium. A comparison of the modes is presented in the bottom-left.

$$v_{qS}(\theta) = \sqrt{\frac{C_{11}\sin^2(\theta) + C_{33}\cos^2(\theta) + C_{44} - \sqrt{M(\theta)}}{2\rho}},$$
$$v_S(\theta) = \sqrt{\frac{C_{66}\sin^2(\theta) + C_{44}\cos^2(\theta)}{\rho}}, \tag{1}$$

with

$$M(\theta) = \left[(C_{11} - C_{44})\sin^2(\theta) - (C_{33} - C_{44})\cos^2(\theta)\right]^2 + (C_{13} + C_{44})\sin^2(2\theta).$$

In Eq. (1) the involved parameters correspond to those indicated in Fig. 1 and defining the elastic stiffness tensor (C_{IJ}) as per Eq. (2)

$$C = \begin{bmatrix} C_{11} & C_{12} & C_{13} & 0 & 0 & 0 \\ C_{12} & C_{11} & C_{13} & 0 & 0 & 0 \\ C_{13} & C_{13} & C_{33} & 0 & 0 & 0 \\ 0 & 0 & 0 & C_{44} & 0 & 0 \\ 0 & 0 & 0 & 0 & C_{44} & 0 \\ 0 & 0 & 0 & 0 & 0 & C_{66} \end{bmatrix}, \tag{2}$$

with $C_{66} = (C_{11} - C_{12})/2$.

The material parameters are expected to play a fundamental role in the dispersive behavior of the material as clearly observed from the dispersion equations. These relations combine the angle of propagation θ measured with respect to the axis of symmetry, and the 5 material constants appearing in (2). In addition, there are also two other relevant aspects of these relations. First, the purely shear mode has the shape of an ellipsoid with semi-axes $\sqrt{C_{66}/\rho}$ and $\sqrt{C_{44}/\rho}$, which implies that there is a limited degree of directional behavior for this mode. Second, the qP and qS modes are strongly coupled through the term $M(\theta)$ and different combinations of the material parameters may produce strongly different directional behavior. This directional dependence of the phase speed is clarified in Fig. 2, which shows the directionality curve and phase speed surface for magnesium. The difference in the level of anisotropy in the purely shear and the qS and qP modes is evident. In this material the particular values of the elastic parameters are such that the directional effect is stronger in the S and qS modes, while the qP mode remains nearly isotropic (i.e., approaching a sphere). The directional dependence is also shown by the directionality curve for the different modes (shown in the left part of the figure), where the propagation direction is described with respect to the axis of symmetry. Additional cases corresponding to different transversely isotropic materials are included in Table 1.

The directionality curves and the phase speed surfaces showing the ability of the material to propagate mechanical waves in infinite directions can be used as a qualitative description of the level of anisotropy in transversely isotropic materials. In the current work, we have used this idea to compare a database of commonly encountered man-made and natural transversely isotropic materials. The comparison is tabulated in Fig. 3 in which the absolute values for the different speeds are normalized by the maximum for each material to produce an objective qualitative comparison across materials. This qualitative description of anisotropy can, therefore, be used as a first-hand guide in the selection of anisotropic materials.

We observe that in materials like Glass-epoxy, there is a marked directional behavior in the qS mode, while the qP mode remains closely isotropic. However, there is a trend for these modes to propagate at larger speeds along the horizontal direction.

Table 1
Mechanical properties for the considered transversely isotropic materials (Payton, 1983; Nayfeh, 1995; Liu and Xi, 2001; Wagner and Pruß, 2002; Freund and Suresh, 2004). The directionality curves for the list are presented in Fig 3.

Material	C_{11} (GPa)	C_{12} (GPa)	C_{13} (GPa)	C_{33} (GPa)	C_{44} (GPa)	Density (kg/m^3)
Apatite	167	13.1	66	140	66.3	3190
Beryllium	291.25	26.7	14	336.2	162.25	1850
Beryl	282	99.4	69.5	248	68.6	2640
Cadmium	115.9	41.05	41	51.2	19.95	8650
Cobalt	307	165	103	358.05	76.9	8900
Ice (257 K)	13.5	6.5	5.2	14.5	3.17	919
Hafnium	181	77	66	196.95	55.7	13,310
Magnesium	59.2	25.95	21.55	61.4	39.05	1738
Rhenium	612	270	206	683	162	21,200
Titanium	162.2	92	69	180.85	46.7	4506
Thallium	40.8	35.4	29	52.8	7.26	11,850
Yttrium	77.9	29.2	20	76.9	24.31	4472
Zinc	163	32.6	50.05	61.5	38.95	7140
Graphite-epoxy	16.34	4.96	3.72	155.43	7.48	1600
Carbon-epoxy	12.372	6.147	6.185	146.302	4.795	1900
Glass-epoxy	13.475	7.259	6.033	42.001	3.414	2660
Zirconium	143.4	72.8	65.3	164.8	32	6520
ZnO	209.7	121.1	105.1	210.9	42.5	5606

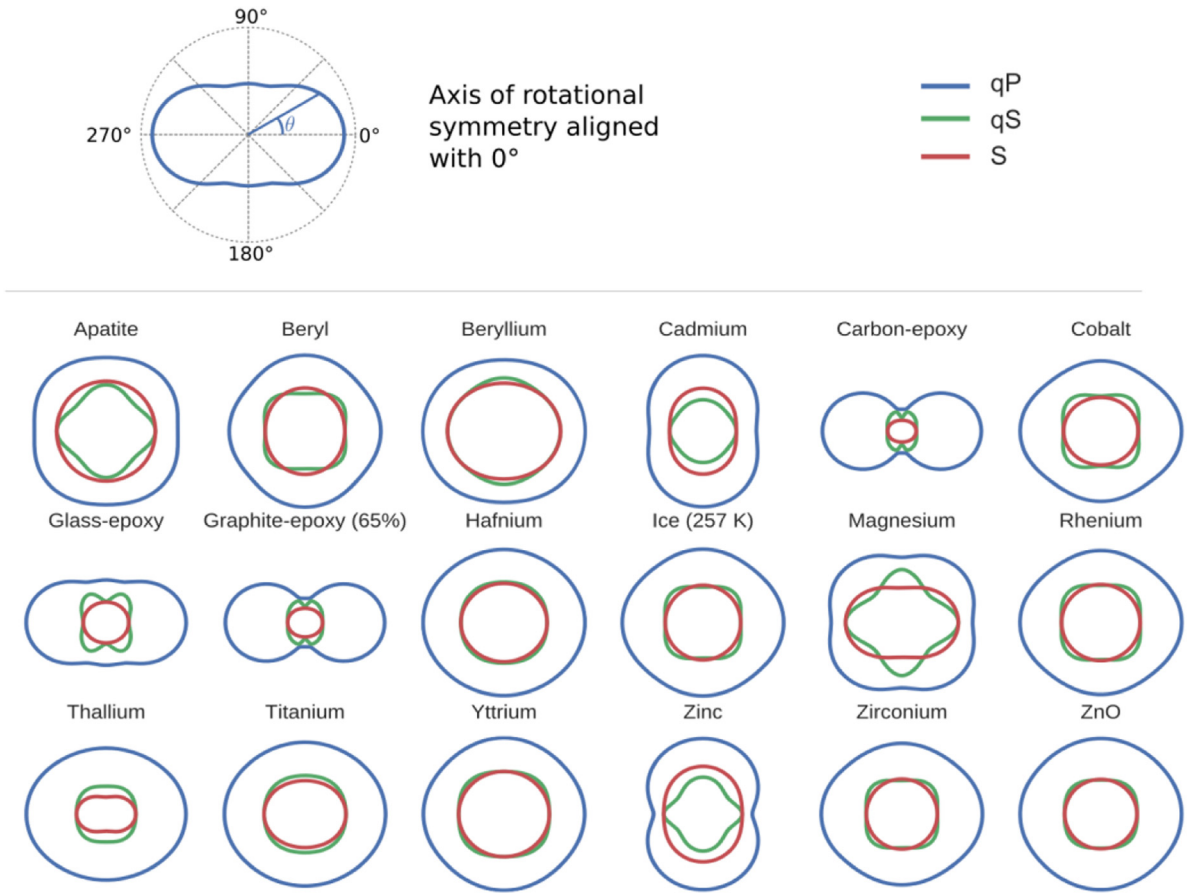

Fig. 3. Directionality curves for different transversely isotropic materials. Blue represents the qP wave, green represents the qS wave, and red represents the S wave. (For interpretation of the references to color in this figure legend, the reader is referred to the web version of this article.)

2.2. Wave directionality and anisotropy index

From an intuitive perspective, it is natural to expect that materials with stronger anisotropy, or equivalently, with a stronger impedance contrast will exhibit larger bandgaps. In this section, we introduce a quantitative description of the level of anisotropy associated with a given material in order to establish an objective criterion for its selection. For this purpose, we need to consider an objective index or measure of the level of anisotropy that takes into account the different phases in these materials.

The simplest quantitative measure of anisotropy is Zener's ratio (Zener, 1948), which is a dimensionless number used to characterize the anisotropy for cubic crystals. Intuitively, it is the ratio between the shear modulus for the cubic material and its isotropic counterpart. In terms of the constitutive constants defined in Eq. (2), this ratio can be written like

$$a_r = \frac{2(1+\upsilon)G}{E} \equiv \frac{2C_{44}}{C_{11}-C_{12}} = \frac{C_{44}}{C_{66}}. \tag{3}$$

Zener ratio takes the value of 1 when the material is isotropic and decreases in the direction of increasing anisotropy. Although Zener's ratio completely quantifies anisotropy for cubic materials, it fails for other material symmetries such as transverse isotropy, which are described by five material parameters.

Kanit et al. (2006) extended Zener's ratio for more general anisotropic materials while keeping a form resembling that in Zener's (Kanit et al., 2006). In this alternative form the terms are now replaced by different averages of the moduli as follows:

$$a_{\text{gen}} = \frac{2Y_{44}}{Y_{11}-Y_{12}}, \tag{4}$$

with

$$Y_{11} = \frac{C_{11}+C_{22}+C_{33}}{3}, Y_{12} = \frac{C_{12}+C_{23}+C_{13}}{3},$$
$$Y_{44} = \frac{C_{44}+C_{55}+C_{66}}{3}. \tag{5}$$

As stated in (5), Y_{11} is the average of the diagonal terms in the stiffness tensor related to axial stresses, Y_{12} is the average of the off-diagonal terms in the stiffness tensor related to axial stresses, and Y_{44} is the average of the diagonal terms related to the shear stresses. This ratio indeed quantifies anisotropy, but it fails to differentiate between different propagation modes for waves.

Casadei and Rimoli (2013) introduced a third anisotropy index (AI) considering each propagation mode and obtained from the corresponding dispersion relation separately. The index is computed as

$$AI = \sqrt{\frac{1}{2\pi}\int_0^{2\pi}\left(\frac{c(\theta)-\bar{c}}{\bar{c}}\right)^2 d\theta}, \tag{6}$$

where $\bar{c}$ is the average speed for all the angles, and $c(\theta)$ is the speed for a direction forming an angle θ with the axis of symmetry. This measure is, essentially, the standard deviation for each wave propagation mode.

In the case of S polarization, the integral for the average speed becomes

$$\overline{c_S} = \frac{2}{\pi}\sqrt{\frac{C_{44}}{\rho}}E\left(1-\frac{C_{66}}{C_{44}}\right), \tag{7}$$

resulting in the following particular form for the anisotropy index AI

$$AI_S = \sqrt{\frac{1}{8}\left[\frac{\pi^2(a_r+1)}{a_r E^2\left(\frac{a_r-1}{a_r}\right)}-8\right]}, \tag{8}$$

where a_r corresponds to Zener's ratio (see Eq. (3)), and E(•) is the complete elliptic integral of the second kind (Olver and Saunders, 2016). For the qS and qP modes the integrals do not have a closed form and need to be computed numerically.

Fig. 4 compares the materials listed in Table 1 in terms of its anisotropy index as per Eq. (6). The directionality curve for each material has also been superimposed for clarity. Common composites like carbon-epoxy or graphite-epoxy present high anisotropy in the qP mode, but not as high for the qS and S modes. On the other hand, in materials like magnesium and thallium, the larger anisotropy is related to the S mode.

2.3. Constituent materials for potential helicoidal architecture

The characterization of transversely isotropic materials in terms of the anisotropy index was used as the basis for the selection of prototype materials to be used in the helicoidal architecture. We selected material 1 to share its properties with carbon-epoxy with a modulus and mass density corresponding to $C_{11} = 12.372$ GPa, $C_{12} = 6.147$ GPa, $C_{13} = 6.185$ GPa, $C_{33} =$

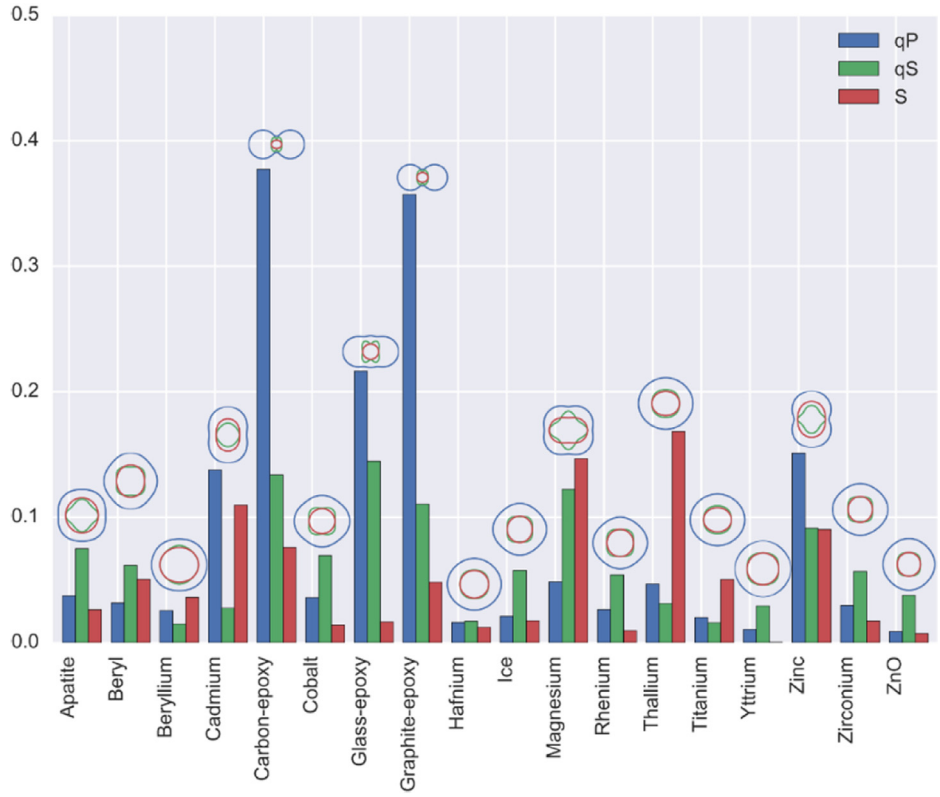

Fig. 4. Anisotropy index from Casadei and Rimoli (2013) for different transversely isotropic materials. Blue represents the qP wave, green represents the qS wave and red represents the S wave. Directionality curves are superimposed for each material to add a qualitative and more intuitive way of comparison. (For interpretation of the references to color in this figure legend, the reader is referred to the web version of this article.)

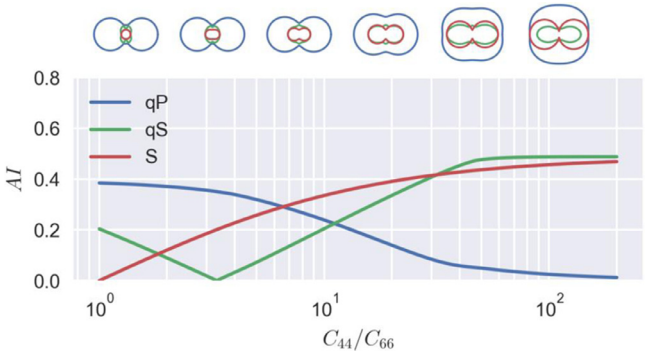

Fig. 5. Anisotropy index for Material 1 while the C_{44} component changes with the other components remaining the same. Blue represents the quasi–P wave, green represents the quasi–S wave and red represents the S wave. In the top we show the directionality curves as a qualitative comparison. (For interpretation of the references to color in this figure legend, the reader is referred to the web version of this article.)

146.302 GPa, $\rho = 1900\,\mathrm{kg/m^3}$, and material 2 with base properties corresponding to those in magnesium with specific values of $C_{11} = 59.2\,\mathrm{GPa}$, $C_{12} = 25.95\,\mathrm{GPa}$, $C_{13} = 21.55\,\mathrm{GPa}$, $C_{33} = 61.4\,\mathrm{GPa}$, $\rho = 1738\,\mathrm{kg/m^3}$. Carbon-epoxy was selected due to its man-made origin while magnesium had merit in the fact that its directionality curves exhibit higher anisotropies for S and qS waves.

To study the directionality in these materials, we varied the C_{44} component of the stiffness tensor, while keeping the other components constant. Figs. 5 and 6 present the variation in the anisotropy index (AI) for different ratios $C_{44}/C_{66} = 2C_{44}/(C_{11} - C_{12})$ in materials 1 and 2, respectively.

Interestingly, in material 1, with prototype given by carbon-epoxy, the anisotropy of the qP mode changes in a direction opposite to the S and qS modes. Apparently, this behavior is only slightly observed in material 2, however it is important to notice that the anisotropy index for both materials is exactly the same since its only dependence is on C_{44}/C_{66}, as shown

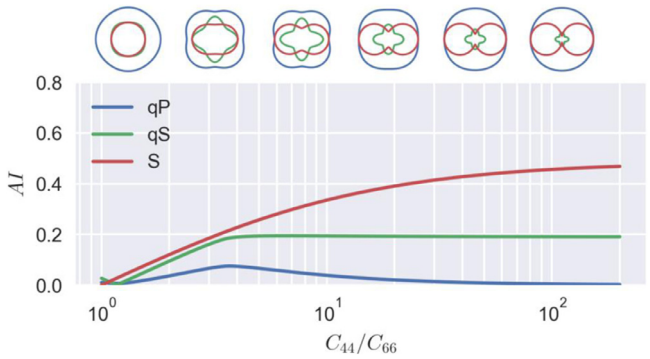

Fig. 6. Anisotropy index for Material 2 while the C_{44} component changes with the other components remaining the same. Blue represents the quasi–P wave, green represents the quasi–S wave and red represents the S wave. In the top we show the directionality curves as a qualitative comparison. (For interpretation of the references to color in this figure legend, the reader is referred to the web version of this article.)

by Eq. (8). Anisotropy for the qS and qP modes depends on other material constants. Nevertheless, the same trends can be seen, i.e., the anisotropy index for qS waves increases and reaches a maximum value, while the anisotropy index for the qP waves decreases.

3. A bioinspired helicoidal composite with transverse isotropy

The analysis conducted in the previous section based upon dispersion curves suggests that the anisotropy level for the S and qS modes is highly sensitive to changes in the C_{44}/C_{66} ratio. In this section, we assume that materials 1 and 2 are used as base materials in the fabrication of helicoidal composites. As described previously, helicoidal architectures are known to exhibit shear wave filtering capabilities and interest now lies in examining the outcome from a combination of transverse isotropy with a helicoidal microstructure. This idea is inspired by results of previous studies aimed at identifying the mechanisms responsible for the remarkable energy dissipation capabilities present in the dactyl club from the Stomatopod. As shown in Guarín–Zapata et al. (2015) its helicoidal microstructure results in shear wave filtering over specific frequency ranges or bandgaps. In this work, we extend upon this idea and explore the impact of producing helicoidal composites whose base materials are transversely isotropic with varying C_{44}/C_{66} ratios. In this analysis, performance is characterized in terms of the band structure of the resulting material which is determined after assuming a unit cell subjected to Bloch periodic boundary conditions. For each material type, we then modify the C_{44}/C_{66} ratio and measure the size of the first bandgap in the corresponding structure diagram. In addition, we provide details about the layered model and the band structure determination.

3.1. Helicoidal composite modeling

A composite with the helicoidal architecture consists of individual layers made of transversely isotropic materials that are piled up in a way that the symmetry axis is rotated from a layer to the next one by a pitch angle, α, in a helicoidal manner. Each layer is considered to behave elastically and to have thickness d. The material is considered to be periodic in the z-direction, and it can be fully described by a single unit cell. Each unit cell contains N layers with a total thickness $D = N \cdot d$; in that way, the first and last layer in a unit cell represents a complete rotation of 180° Fig. 7 depicts a schematic of the helicoidal composite and its unit cell. The rotation between two consecutive layers affects the constitutive tensor in Eq. (B1), which translates in an impedance contrast for shear waves but does not have an effect in longitudinal ones. Similarly, for the specific case of composites, the stiffness mismatch between the fibers and the matrix and the fiber volume fraction controls the anisotropy, and therefore the directionality of the composite.

As the composite material is organized in a series of stacked layers, we can express the solution through a product of propagation matrices (Gilbert and Backus, 1966). This allows us to transform the equations of motion into a system of Ordinary Differential Equations (ODEs) (Yang et al., 1991; Guarín–Zapata et al, 2015). Furthermore, the utilization of Bloch's theorem translates the ODE problem into an eigenvalue one (Deymier, 2013; Hussein et al., 2014):

$$[Q(\omega)]V = \mathrm{e}^{-ikD}V, \tag{9}$$

the form of the matrix $[Q(\omega)]$ is presented in Appendix B.

Solving this eigenvalue problem for a series of frequencies (ω) enables us to construct the dispersion relations and, as a consequence, the overall behavior of the helicoidal material (Kittel and McEuen, 1986; Brillouin, 2003). The magnitude of the eigenvalues, e^{-ikD}, informs if a wave mode propagates ($|\mathrm{e}^{-ikD}| = 1$) or not, meaning there is a bandgap ($|\mathrm{e}^{-ikD}| \neq 1$). In the case of non-propagating waves, this magnitude can represent the decaying factor between two consecutive cells (Hochstadt, 1975).

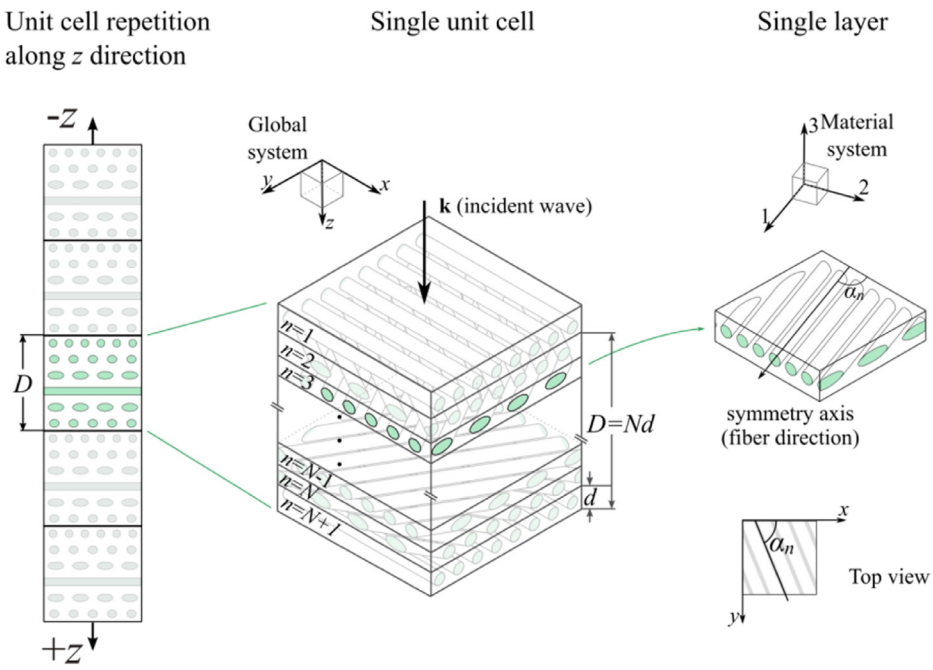

Fig. 7. Schematic of the helicoidal composite (adapted from Guarín–Zapata et al., 2015). The material repeats periodically in the z direction with period D. The unit cell consists of individual layers with unidirectional fibers that are rotated by an angle α with respect to the previous one. Thus, the orientation of the nth layer is given by $\alpha_n = (n-1)\,\alpha$. Each of the layers is modeled as a transversely isotropic material of thickness d.

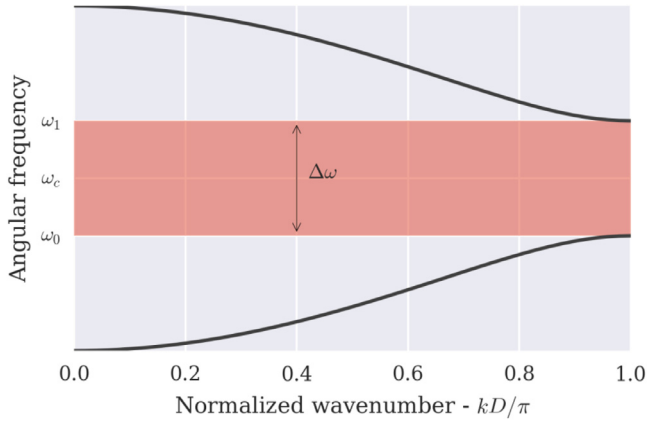

Fig. 8. Schematic of the first bandgap, and its size. The gap-midgap ratio results after dividing the gap size by its central value as per Eq. (10).

3.2. Bandgap size

To qualify the performance of the combinations of the C_{44}/C_{66} ratio with the different geometric parameters of the unit cell, we use the size of the first bandgap as a figure of merit. Nevertheless, since the first band gap might appear at higher or lower frequencies, it is customary to use the gap–midgap ratio (Joannopoulos et al., 2011) as it provides a comparison that is not subject to the scaling given by changes in the material constants. It is explicitly written as:

$$\frac{\Delta\omega}{\omega_c} \equiv \frac{\omega_1 - \omega_0}{\omega_c}, \tag{10}$$

with the involved parameters illustrated in Fig. 8. Thus, we expect a specific combination of material and geometric parameters to be considered highly effective if it results in a wider bandgap.

As indicated previously, we varied the C_{44} component of the stiffness tensor, while keeping the other components constant. This increase in the C_{44}/C_{66} ratio leads to an increase in the size of the bandgaps as shown in Figs. 9 and 10, where we plotted the size of the bandgap as a function of C_{44}/C_{66} for helicoidal composites with different pitch angles (α). As expected, the introduction of transversely isotropic materials in the helicoidal architecture increases the size of the bandgap.

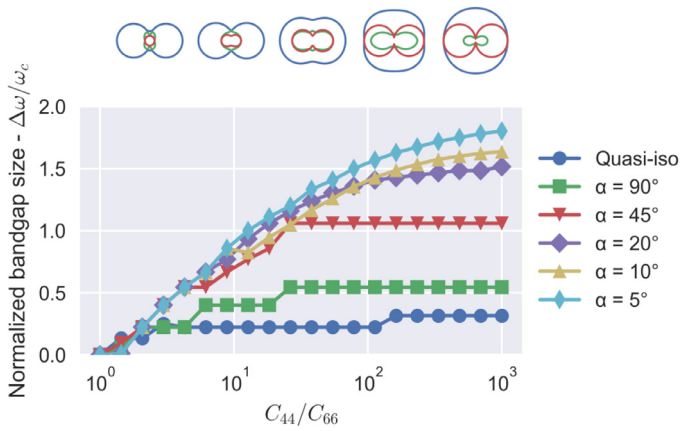

Fig. 9. Size of the first bandgap vs. C_{44}/C_{66} ratio for helicoidal composites made with Material 1 with different pitch angles (α). For comparison we also computed the values for quasi-isotropic composites (Quasi–iso).

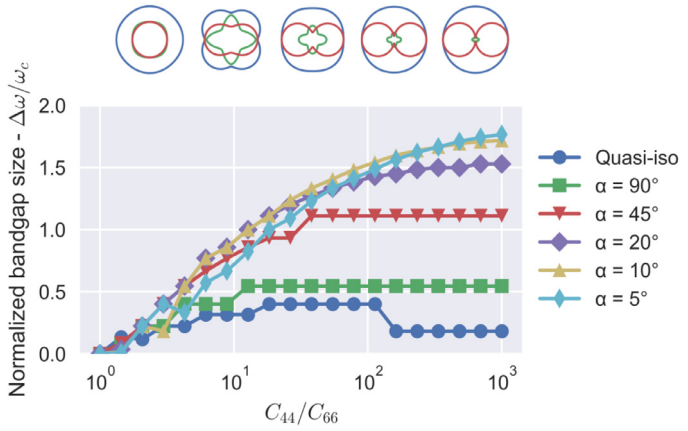

Fig. 10. Size of the first bandgap vs. C_{44}/C_{66} ratio for helicoidal composites made with Material 2 with different pitch angles (α). For comparison we also computed the values for quasi-isotropic composites (Quasi–iso).

This result can be verified after comparing the size of the bandgap for a quasi-isotropic material (also shown in the figures) with those corresponding to the current prototypes. Moreover, the size of the bandgap remains nearly constant in the quasi-isotropic (quasi-iso) case while it shows significant increments for the transversely isotropic materials. At the same time, it is observed that how this gain in bandgap size is stronger at small values of the pitch angle as revealed by the curves corresponding to pitch angles of 45° and below. For different C_{44}/C_{66} values, the qualitative shape of the different propagation modes undergoes small sudden variations as it can be observed on the upper part of Figs. 9 and 10. The sequence of images shows how the wave propagation modes can have a different number of inflection points and cusps depending on the ratio C_{44}/C_{66} (Payton 1983).

To understand the influence of varying the mechanical properties in transversely isotropic material in helicoidal architectures in dynamic impact problems, we evaluated the filtering capabilities of the material for impact events represented by a square pulse. This is measured using the ratio between the transmitted energy and the total energy of the pulse (Guarín-Zapata et al., 2015). The duration of the pulse is $C_{11}\Delta t/\rho d = 1$, and the selection of a square shape in the time domain translates into a wide Fourier spectrum involving higher harmonics. The transmitted energy is the one that does not overlap with the bandgap. In Fig. 11, this is the region outside the range ω_0–ω_1, and it is described by the following expression:

$$E_{\text{trans}} = \frac{2}{K}\left[\int_0^{\omega_0} |\sigma(\omega)|^2 d\omega + \int_{\omega_1}^{\infty} |\sigma(\omega)|^2 d\omega\right] \tag{11}$$

where K is a material constant that guarantees that the units are consistent.

As mentioned above, we compared the ratio between the transmitted energy (E_{trans}) and the total energy (E_{total}), denoted by η, which is given by:

$$\eta = \frac{E_{\text{trans}}}{E_{\text{total}}} \tag{12}$$

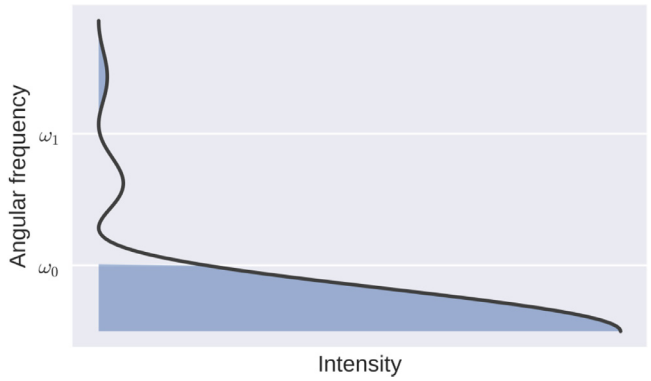

Fig. 11. Schematic for the frequency ranges of transmitted and filtered energy. The shaded region depicts the transmitted energy while the range between ω_0 and ω_1 is the filtered energy.

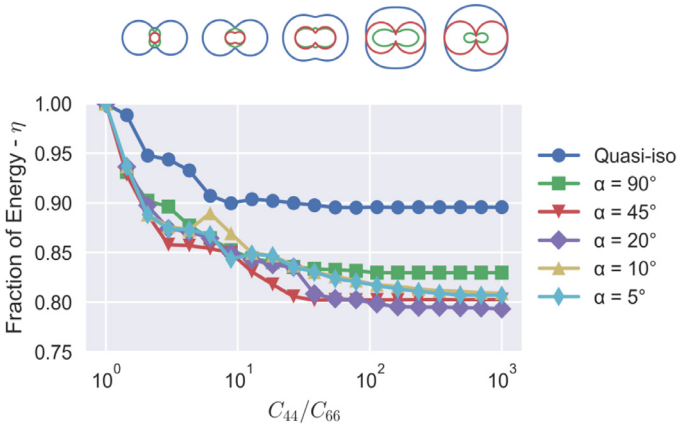

Fig. 12. Fraction of transmitted energy vs. C_{44}/C_{66} for helicoidal composites made with Material 1 with different pitch angles (α). For comparison we also computed the values for quasi-isotropic composites (Quasi–iso).

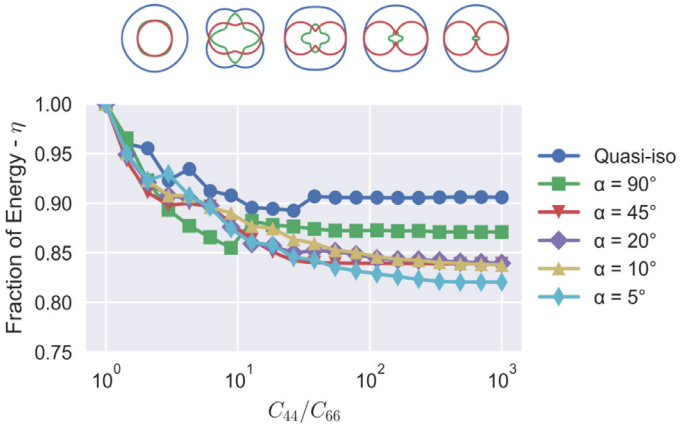

Fig. 13. Fraction of transmitted energy vs. C_{44}/C_{66} for helicoidal composites made with Material 2 with different pitch angles (α). For comparison we also computed the values for quasi-isotropic composites (Quasi–iso).

Figs. 12 and 13 present the fraction of transmitted energy for the two base materials studied when changing the C_{44}/C_{66} ratio for helicoidal composites with different pitch angles (α), and they are compared with the case of a quasi-isotropic composite.

These results lead us to conclude that we can control the size of bandgaps for shear waves by controlling the value of the component C_{44} of the stiffness tensor. To achieve this goal, we would need to design the material with a specific constitutive tensor in mind, i.e., find the microstructure that allows a ratio C_{44}/C_{66} that gives us the desired dispersion characteristics—

like the gap–midgap ratio. The problem of obtaining an elastic material with a set of desired parameters has been studied from a theoretical point of view (Milton and Cherkaev, 1995), and some interesting results have been achieved (Norris and Nagy, 2011). Besides the theoretical approach to this inverse problem, there have been different topological optimization approaches to the design of microstructures to obtain the desired properties of a material (Bendsoe and Sigmund, 2013; Liu et al.; 2016).

4. Conclusions

We studied the dispersion of waves propagating in helicoidal layered composites using the propagation matrix formalism and the Bloch theorem to represent periodicity of the material. We considered the anisotropic behavior of a collection of transversely isotropic materials, and presented a qualitative and quantitative way to represent their anisotropy (directionality). From this collection of materials, we selected carbon-epoxy and magnesium, a man-made material and a natural occurring material with anisotropic behavior, as base materials to analyze the effect of modifying the C_{44} component of the stiffness tensor in wave dispersion. We found, for hypothetical materials that share the rest of their elastic properties with carbon–epoxy or magnesium, that the directionality of the S wave increases along with the ratio C_{44}/C_{66}. We analyzed, as well, the wave dispersion in helicoidal layered composites constituted of these hypothetical transversely isotropic materials, i.e., materials with different anisotropy levels. We observed that the normalized size of the first bandgap grows with increasing C_{44}/C_{66}, and that is largest for the smallest pitch angle considered (5°). The results show that the most important parameter for shear wave filtering is the ratio of the constants C_{44}/C_{66}. Hence, in the design of layered composites with desired appearance and size of bandgaps, the anisotropy of the S waves in each layer is more interesting than the anisotropy for quasi-S and quasi-P ones.

Acknowledgments

We would like to acknowledge financial support from the National Science Foundation through the CAREER award CMMI 1254864, the Air Force Office of Scientific Research (AFOSR-FA9550-12-1-0245) and the Multi-University Research Initiative (MURI AFOSR-FA9550-15-1-0009). PZ acknowledges initial discussions and collaboration with Dr. G. Milliron.

Supplementary materials

Supplementary material associated with this article can be found, in the online version, at doi:10.1016/j.jmps.2019.07.003.

Appendix A. Wave propagation in materials with transverse isotropy

Throughout this section, Einstein notation is used. Hence, repeated indices imply a sum and a comma denotes differentiation.

Newton's second law for an elastic solid without body forces gives the following equation of motion:

$$\sigma_{ij,i} = \rho \frac{\partial^2 u_j}{\partial t^2}, \tag{A1}$$

with u_j, σ_{ij} and ρ the displacement, stress tensor and density, respectively. Furthermore, the material is considered to satisfy the Hooke's law as constitutive relationship,

$$\sigma_{ij} = c_{ijpq} u_{p,q}\,, \tag{A2}$$

where c_{ijpq} is the stiffness tensor that in the case of transversely isotropic materials is formed with 5 different parameters (Payton, 1983). . We assume a solution in the form of a plane wave:

$$u_j = U_j \exp[ik(n_r x_r - v_p t)]\,, \tag{A3}$$

where k is the wavenumber, n_r is a unit vector in the direction of propagation, and v_p is the phase velocity. Assuming a harmonic behavior, plugging (A2) and (A3) to (A1) gives the Christoffel wave equation (Buchwald, 1959; Auld, 1973; Carcione, 2001),

$$\left[\Gamma_{ij} - \rho\, {v_p}^2 \delta_{ij}\right] U_j = 0\,, \tag{A4}$$

where $\Gamma_{ij} = c_{ijkl} n_k n_l$ is the Christoffel stiffness tensor, and δ_{ij} is the Kronecker delta. Since we are not interested in null solutions, thus we force the determinant to be zero,

$$\det\left[\Gamma_{ij} - \rho\, {v_p}^2 \delta_{ij}\right] = 0\,. \tag{A5}$$

The solutions of this characteristic polynomial give rise to the different modes of propagation in the medium (Auld, 1973; Carcione, 2001). One of the propagation modes presents transverse polarization, while the other two present quasi-tranverse and quasi-longitudinal polarizations. Eq. (A5) depends on the direction of propagation. This implies that the phase velocities depend on the direction of propagation of the wave.

Appendix B. Matrices for a single layer and for a unit cell

The propagation matrix [P] that relates the state vector between two consecutive layers is given by ():

$$[P] = \begin{bmatrix} 0 & 0 & k_x & \frac{-iC_{44}}{\Delta} & \frac{-iC_{45}}{\Delta} & 0 \\ 0 & 0 & 0 & \frac{-iC_{45}}{\Delta} & \frac{-iC_{55}}{\Delta} & 0 \\ \frac{k_x C_{13}}{C_{33}} & \frac{k_x C_{36}}{C_{33}} & 0 & 0 & 0 & \frac{-i}{C_{33}} \\ A & B & 0 & 0 & 0 & \frac{k_x C_{13}}{C_{33}} \\ B & M & 0 & 0 & 0 & \frac{k_x C_{36}}{C_{33}} \\ 0 & 0 & i\rho\omega^2 & k_x & 0 & 0 \end{bmatrix}, \tag{B1}$$

with

$$A = i\left[\rho\omega^2 - \left(C_{11} - \frac{C_{13}C_{13}}{C_{33}}\right)k_x^2\right], \tag{B2}$$

$$M = i\left[\rho\omega^2 - \left(C_{66} - \frac{C_{36}C_{36}}{C_{33}}\right)k_x^2\right], \tag{B3}$$

$$B = -i\left(C_{16} - \frac{C_{13}C_{36}}{C_{33}}\right)k_x^2, \tag{B4}$$

$$\Delta = C_{44}C_{55} - C_{45}^2. \tag{B5}$$

The matrix [$Q(\omega)$] that presents geometric and material information of the composite is given by:

$$[Q(\omega)] = e^{id_N[P_N(\omega)]}e^{id_{N-1}[P_{N-1}(\omega)]}\dots e^{id_1[P_1(\omega)]}, \tag{B6}$$

it should be noted that both the matrix [P] and the matrix [Q] depend on the frequency, geometry and material properties.

References

Akbari, S., Sakhaei, A.H., Kowsari, K., Yang, B., Serjouei, A., Yuanfang, Z., Ge, Q., 2018. Enhanced multimaterial 4D printing with active hinges. Smart Mater. Struct. 27 (6), 065027.

Al-Sawalmih, A., Li, C., Siegel, S., Fabritius, H., Yi, S., Raabe, D., Fratzl, P., Paris, O., 2008. Microtexture and chitin/calcite orientation relationship in the mineralized exoskeleton of the American lobster. Adv. Funct. Mater. 18, 3307–3314.

Ashby, M.F., Bréchet, Y.J.M., 2003. Designing hybrid materials. Acta Mater. 51 (19), 5801–5821.

Astaneh, A.V., Guddati, M.N., 2017. Dispersion analysis of composite acousto-elastic waveguides. Compos. Part B 130, 200–216.

Auld, B.A., 1973. Acoustic Fields and Waves in Solids. Wiley, New York.

Babaee, S., Shim, J., Weaver, J.C., Chen, E.R., Patel, N., Bertoldi, K., 2013. 3D Soft metamaterials with negative Poisson's ratio. Adv. Mater. 25, 5044–5049.

Backus, G.E., 1962. Long-wave elastic anisotropy produced by horizontal layering. J. Geophys. Res. 67 (11), 4427–4440.

Barthelat, F., 2007. Biomimetics for next generation materials. Philos. Trans. R. Soc. Lond. A 365 (1861), 2907–2919.

Bendsoe, M.P., Sigmund, O., 2013. Topology Optimization: Theory, Methods, and Applications. Springer Science & Business Media.

Brechet, Y., Embury, J.D., 2013. Architectured materials: expanding materials space. Scr. Mater. 68 (1), 1–3.

Brillouin, L., 2003. Wave Propagation in Periodic structures: Electric Filters and Crystal Lattices. Courier Dover Publications.

Buchwald, V., 1959. Elastic waves in anisotropic media. Proc. R. Soc. Lond. Ser. A. Math. Phys. Sci. 253, 563–580.

Carcione, J.J.M., 2001. Wave Fields in Real Media: Wave Propagation in Anisotropic, Anelastic and Porous Media. Pergamon.

Casadei, F., Rimoli, J., 2013. Anisotropy-induced broadband stress wave steering in periodic lattices. Int. J. Solids Struct. 50, 1402–1414.

Celli, P., Gonella, S., 2015. Manipulating Waves with LEGO ® Bricks: a Versatile Experimental Platform for Metamaterial Architectures. arXiv:1505.04456.

Chen, P.-Y., Lin, A.Y.-M., McKittrick, J., Meyers, M.A., 2008. Structure and mechanical properties of crab exoskeletons. Acta Biomater. 4, 587–596.

Cheng, L., Wang, L., Karlsson, A.M., 2008. Image analyses of two crustacean exoskeletons and implications of the exoskeletal microstructure on the mechanical behavior. J. Mater. Res. 23, 2854–2872.

Cheng, L., Wang, L., Karlsson, A.M., 2009. Mechanics-based analysis of selected features of the exoskeletal microstructure of Popillia japonica. J. Mater. Res. 24, 3253–3267.

Cheng, L., 2010. Mechanical Implications of the Arthropod Exoskeleton Microstructures and the Mechanical Behavior of the Bioinspired Composites.

Deymier, P.A. (Ed.), 2013. Acoustic metamaterials and phononic crystals, Springer Series in Solid-State Sciences, first ed. Springer.

Dvorak, G.J., 2013. Tensor Component and Matrix Notations. In: Micromechanics of Composite Materials. Springer, Dordrecht, pp. 1–9.

Freund, L.B., Suresh, S., 2004. Thin Film materials: stress, Defect Formation and Surface Evolution. Cambridge University Press.

Ge, Q., Qi, H.J., Dunn, M.L., 2013. Active materials by four-dimension printing. Appl. Phys. Lett. 103, 131901.

Gibson, R.F., 2011. Principles of Composite Material Mechanics. CRC Press.

Gilbert, F., Backus, G.E., 1966. Propagator matrices in elastic wave and vibration problems. Geophysics 31, 326–332.

Grunenfelder, L., Suksangpanya, N., Salinas, C., Milliron, G., Yaraghi, N., Herrera, S., Evans-Lutterodt, K., Nutt, S., Zavattieri, P., Kisailus, D., 2014. Bio-inspired impact resistant composites. Acta Biomater. 10, 3997–4008.

Grunenfelder, L.K., Milliron, G, Herrera, S., Gallana, I., Yaraghi, N., Hughes, N., Evans-Lutterodt, K., Zavatttieri, P., Kisailus, D., 2018. Ecologically driven ultrastructural and hydrodynamic designs in stomatopod cuticles. Adv. Mater. 30 (9), 1705295.

Guarín–Zapata, N., Gomez, J., Yaraghi, N., Kisailus, D., Zavattieri, P.D., 2015. Shear wave filtering in naturally–occurring Bouligand structures. Acta Biomaterialia..

Hochstadt, H., 1975. Differential equations: a Modern Approach. Courier Dover Publications.

Huang, W., Restrepo, D., Jung, J.-Y., Su, F.Y., Liu, Z., Ritchie, R.O., McKittrick, J., Zavattieri, P., Kisailus, D., 2019. Multiscale toughening mechanisms in biological materials and bioinspired designs. Adv. Mater. doi:10.1002/adma.201901561.

Hussein, M.I., Leamy, M.J., Ruzzene, M., 2014. Dynamics of phononic materials and structures: Historical origins, recent progress, and future outlook. Appl. Mech. Rev. 66, 040802.

Jasiuk, I., Abueidda, D.W., Kozuch, C., Pang, S., Su, F.Y., McKittrick, J., 2018. An overview on additive manufacturing of polymers. JOM 70 (3), 275–283.

Joannopoulos, J.D., Johnson, S.G., Winn, J.N., Meade, R.D., 2011. Photonic crystals: Molding the Flow of Light. Princeton university press.

Jones, R.M., 1975. Mechanics of Composite Materials. Scripta Book Company, Washington, DC.
Kanit, T., N'Guyen, F., Forest, S., Jeulin, D., Reed, M., Singleton, S., 2006. Apparent and effective physical properties of heterogeneous materials: Representativity of samples of two materials from food industry. Comput. Meth. Appl. Mech. Eng. 195, 3960–3982.
Kittel, C., McEuen, P., 1986. Introduction to Solid State Physics. Wiley, New York.
Liang, Y., Li, Y, Liu, Y., Han, Q., Liu, D., 2018. Investigation of wave propagation in piezoelectric helical waveguides with the spectral finite element methodology. Compos. Part B doi:10.1016/j.compositesb.2018.09.083.
Lin, E., Li, Y., Ortiz, C., Boyce, M.C., 2014. 3D printed, bio-inspired prototypes and analytical models for structured suture interfaces with geometrically-tuned deformation and failure behavior. J. Mech. Phys. Solids 73, 166–182.
Liu, G.R., Xi, Z.C., 2001. Elastic Waves in Anisotropic Laminates. CRC press.
Liu, Y.-C., Huang, J.H., 2012. Dispersion relations and modes of wave propagation in inclusion-reinforced composite plates. Compos. Part B 43 (3), 1649–1657.
Liu, Z.F., Wu, B., He, C.F., 2016. The properties of optimal two-dimensional phononic crystals with different material contrasts. Smart Mater. Struct. 25 (9), 095036.
Meyers, M.A., McKittrick, J., Chen, P.-Y., 2013. Structural biological materials: critical mechanics-materials connections. Science 339, 773–779.
Milton, G.W., Cherkaev, A.V., 1995. Which elasticity tensors are realizable? J. Eng. Mater. Technol. 117, 483–493.
Moakher, M., 2009. The algebra of fourth-order tensors with application to diffusion MRI. In: Visualization Processing Tensor Fields. Springer, pp. 57–80.
Musgrave, M.J.P., 1970. Crystal Acoustics: Introduction to the Study of Elastic Waves and Vibrations in Crystal. Holden-Day.
Naleway, S.E., Porter, M.M., McKittrick, J., Meyers, M.A., 2015. Structural design elements in biological materials: application to bioinspiration. Adv. Mater. 27, 5455–5476.
Naleway, S.E., Taylor, J.R., Porter, M.M., Meyers, M.A., McKittrick, J., 2016. Structure and mechanical properties of selected protective systems in marine organisms. Mater. Sci. Eng.: C 59, 1143–1167.
Nayfeh, A.H., 1995. Wave Propagation in Layered Anisotropic media: with Application to Composites, 39. Elsevier.
Nikolov, S., Fabritius, H., Petrov, M., Friák, M., Lymperakis, L., Sachs, C., Raabe, D., Neugebauer, J., 2011. Robustness and optimal use of design principles of arthropod exoskeletons studied by ab initio-based multiscale simulations. J. Mech. Behav. Biomed. Mater. 4, 129–145.
Nikolov, S., Petrov, M., Lymperakis, L., Friák, M., Sachs, C., Fabritius, H.-O., Raabe, D., Neugebauer, J., 2010. Revealing the design principles of high-performance biological composites using Ab initio and multiscale simulations: the example of lobster cuticle. Adv. Mater. 22, 519–526.
Norris, A.N., Nagy, A.J., 2011. Metal water: a metamaterial for acoustic cloaking. Proc. Phonon. 112–113.
Nye, J.F., 1985. Physical Properties of crystals: their Representation by Tensors and Matrices. University press, Oxford.
Olver, F.W.J., Olde Daalhuis, A.B., Lozier, D.W., Schneider, B.I., Boisvert, R.F., Clark, C.W., Saunders, B.V. (Eds.), 2016. NIST Digital Library of Mathematical Functions. NIST.
Payton, R.G., 1983. Elastic wave propagation in transversely isotropic media. Monographs and Textbooks of Mechanics of solids: Mechanics of Elastic and Inelastic Solids, 1st ed Martinus Nijhoff Publishers.
Porter, M.M., Ravikumar, N., Barthelat, F., Martini, R., 2017. 3D-printing and mechanics of bio-inspired articulated and multi-material structures. J. Mech. Behav. Biomed. Mater. 73, 114–126.
Saheb, D.N., Jog, J., et al., 1999. Natural fiber polymer composites: a review. Adv. Polym. Technol. 18, 351–363.
Shishehbor, M., Zavattieri, P.D., 2019. Effects of interface properties on the mechanical properties of bio-inspired cellulose nanocrystal (CNC)-based materials. J. Mech. Phys. Solids 124, 871–896.
Slawinski, M.A., 2010. Waves and Rays in Elastic Continua. World Scientific.
Slesarenko, V., Kazarinov, N., Rudykh, S., 2017. Distinct failure modes in bio-inspired 3D-printed staggered composites under non-aligned loadings. Smart Mater. Struct. 26 (3), 035053.
Srivastava, A., 2016. Metamaterial properties of periodic laminates. J. Mech. Phys. Solids 96, 252–263.
Suksangpanya, N., Yaraghi, N.A., Kisailus, D., Zavattieri, P., 2017. Twisting cracks in Bouligand structures. J. Mech. Behav. Biomed. Mater. 76, 38–57.
Suksangpanya, N., Yaraghi, N.A., Pipes, R.B., Kisailus, D., Zavattieri, P., 2018. Crack twisting and toughening strategies in Bouligand architectures. Int. J. Solids Struct. 150, 83–106.
Thierry, V., Brown, L., Chronopoulos, D., 2018. Multi-scale wave propagation modelling for two-dimensional periodic textile composites. Compos. Part B 150, 144–156.
Wagner, W., Pruß, A., 2002. The IAPWS formulation 1995 for the thermodynamic properties of ordinary water substance for general and scientific use. J. Phys. Chem. Ref. Data 31 (2), 387–535.
Weaver, J.C., Milliron, G.W., Miserez, A., Evans-Lutterodt, K., Herrera, S., Gallana, I., Mershon, W.J., Swanson, B., Zavattieri, P., DiMasi, E., et al., 2012. The stomatopod dactyl club: a formidable damage-tolerant biological hammer. Science 336, 1275–1280.
Wegst, U., Ashby, M., 2004. The mechanical efficiency of natural materials. Philos. Mag. 84, 2167–2186.
Willis, J., 2015. Negative refraction in a laminate. J. Mech. Phys. Solids.
Yamamoto, T., Hasegawa, T., Sasaki, M., Hongo, H., Tabata, C., Liu, Z., Li, M., Amizuka, N., 2012. Structure and formation of the twisted plywood pattern of collagen fibrils in rat lamellar bone. J. Electron Microsc. 61, 113–121.
Yang, S.K., Varadan, V.V., Lakhtakia, A., Varadan, V.K., 1991. Reflection and transmission of elastic waves by a structurally chiral arrangement of identical uniaxial layers. J. Phys. D Appl. Phys. 24, 1601.
Yaraghi, N.A., Guarín-Zapata, N., Grunenfelder, L.K., Hintsala, E., Bhowmick, S., Hiller, J.M., Betts, M., Principe, E.L., Jung, J.-Y., Sheppard, L., Wuhrer, R., McKittrick, J., Zavattieri, P.D., Kisailus, D., 2016. Biocomposites: a sinusoidally architected helicoidal biocomposite (Adv. Mater. 32/2016). Adv. Mater. 28 6769–6769.
Yaraghi, N.A., Trikanad, A.A., Restrepo, D., Huang, W., Rivera, J., Herrera, S., Zhernenkov, M., Parkinson, D.Y., Caldwell, R.L., Zavattieri, P.D., Kisailus, D., 2019. The stomatopod telson: convergent evolution in the development of biological shield. Adv. Funct. Mater. doi:10.1002/adfm.201902238.
Zener, C., 1948. Elasticity and Anelasticity of Metals. University of Chicago press.
Zimmermann, E.A., Gludovatz, B., Schaible, E., Dave, N.K., Yang, W., Meyers, M.A., Ritchie, R.O., 2013. Mechanical adaptability of the Bouligand-type structure in natural dermal armour. Nat. Commun. 4, 2634.